

Interaction of Strength and Stress in High, Steep Rock Slopes

John V. Smith¹

¹ School of Engineering, Royal Melbourne Institute of Technology University, Victoria, Australia

Correspondence: John V. Smith, School of Engineering, Royal Melbourne Institute of Technology University, Victoria, GPO Box 2476 Melbourne, Victoria 3001, Australia. Tel: 6-139-9251-298. E-mail: johnv.smith@rmit.edu.au

Received: December 6, 2015

Accepted: December 20, 2015

Online Published: January 6, 2016

doi:10.5539/jgg.v8n1p14

URL: <http://dx.doi.org/10.5539/jgg.v8n1p14>

The research is financed by Royal Melbourne Institute of Technology University.

Abstract

The strength of rock mass and the stress in a slope are each complex fields of investigation. They are also intimately related as increasing confining stress makes a rock mass stronger and the strength of a rock mass can limit the magnitude of stress. Whereas these interactions are comparatively well understood for soils, principally through the advances of laboratory soil mechanics, the scale of rock masses, principally the presence of discontinuity surfaces, limits the capacity for laboratory investigation. The interaction of strength and stress in rock slopes is most evident in high, steep slopes where stress is typically greater. The slope angle and failure mechanisms occurring in the rock slope can reveal the ways that strength and stress interact to produce the observed morphology. McKay Bluff, near Nelson, South Island, New Zealand, is a high, steep rock slope affected by marine coastal erosion at its base. Finite element modeling illustrates sensitivities in determination of the stress magnitude in the slope. Engineering geology methods demonstrate the difficulty in precise determination of the rock mass strength. The ranges of these parameters are compared to find a compatible range for the interacting factors. The stress in a range of other high, steep slope types is reviewed and the implications for geomorphic analysis are discussed.

Keywords: rock slope, stress, rock mass strength, Nelson, New Zealand

1. Introduction

In a review of rock coast geomorphology Naylor, Stephenson, and Trenhaile (2010) noted “modeling would also benefit from collaboration with engineering geologists, who are making considerable progress in our ability to predict how rock masses are likely to erode.” There are also opportunities for engineering geologists to learn from geomorphological approaches to the processes that control the height and steepness of natural slopes. The steepness of rocky coasts, for example, varies such that “near-vertical profiles occur where marine processes are dominant, whereas subaerial erosion tends to smooth and lower the cliff slope” (Kennedy & Dickson, 2007). The shape of naturally formed slopes in rock represents the complex interplay of the strength of rock and the low or high stress conditions to which it is subjected. At a coast this interplay can be driven by erosional undercutting of the slope toe leading to the slope forming its steepest stable slope.

1.1 Strength of Rock

The strength of intact rock samples can be measured in the laboratory. The strength is known to vary according to sample size and according to the confining stress during testing (Paterson & Wong, 2005). The strength of a rock specimen can be measured in confined (such as triaxial) or unconfined (such as uniaxial) conditions. Uniaxial compressive strength (UCS) refers to a standard sample size, shape and standard test conditions – including zero confining stress (ISRM, 1987).

In the field, measuring the strength of rock is a more complex problem as it is characterized by the interaction of intact rock strength and the spacing, orientation, length and frictional properties of discontinuities (together known as rock mass, Wyllie & Mah, 2004). Field mapping of these features can be used to assess the rock mass strength using methods such as the Geological Strength Index (GSI) within the Hoek-Brown rock mass strength model (Hoek & Brown, 1997; Marinos, Marinos, & Hoek, 2005). The Hoek-Brown model treats discontinuities

as being effectively isotropic in distribution and orientation and therefore explicitly excludes the role of problematic structural orientations that are susceptible to kinematic failures such as planar and wedge block sliding (Hoek & Brown, 1997; Marinos et al., 2005).

Many rock slope stability problems are controlled by the kinematics of structures, mainly defects and weaknesses such as joints, bedding, foliation and faults (Wyllie & Mah, 2004; Youssef, 2012). These defects are typically oriented in particular directions such that the rock mass is anisotropic. Therefore the rock mass strength methods alone are insufficient and it is also necessary to analyse stability of structural blocks at the rock slope surface.

The mechanisms of deformation involving surfaces of weakness that allow blocks of rock to separate and fall or slide from a slope can be highly complex (e.g. Alejano, Gómez Márquez, & Martínez Alegría, 2010). Where deformation mechanisms can be inferred accurately, the stability of a slope can be analysed directly by a range of numerical methods (e.g. Stead, Eberhardt, & Coggan, 2006). The important role of discontinuities in the physical erosion of a rock mass has been applied in studies of coastal rock platforms (Naylor & Stephenson, 2010) and the size of coastal boulders (Stephenson & Naylor, 2011). The role of large geological structures such as faults, has been investigated for large landslides (Delgado et al., 2011) and the development of rocky coastal features, cliffs and embankments (Gómez Pujol, Vicente, García Tortosa, Alfaro, Estévez, López Sánchez, & Mallorquí, 2013). In particular, rock mass strength and kinematic slope instability has been shown to be highly influenced by the presence of major faults (Korup, 2004; Brideau, Yan, & Stead, 2009).

1.2 Stress in Slopes

The stability of a slope is typically analysed by assessing the equilibrium of forces in the slope. The balance of driving and resisting forces on an existing or newly formed failure surface leads to a limit-equilibrium analysis (Wyllie & Mah, 2004). This approach is not adequate for high, steep slopes as a clearly defined failure surface does not typically exist or develop, making the assessment of the stability of slopes in strong rocks more problematic than for soils and weak rocks (Wyllie & Mah, 2004).

Stress analysis provides additional important information needed to assess slope stability in high, steep slopes. Stress in a slope can be modeled by use of finite element analysis however, the results are typically highly sensitive to the choice of input parameters. In particular, elastic models do not limit the magnitude of stress and unrealistically high stresses can be found in such models. Where plastic materials are used the stress is limited by the strength of the rock and therefore the derived stress is highly sensitive to the selected strength model (Kinakin & Stead, 2005).

In this paper, the geomorphic and geological factors controlling strength and stress in high, steep rock slopes is illustrated using simple finite element modeling of a relevant field example. The main sensitivities are highlighted to provide general understanding of stress levels in such slopes. The role of stress in geomorphic processes is further illustrated for range of landform profile shapes.

2. Field Example McKay Bluff, New Zealand

2.1 Regional Setting

McKay Bluff is a high coastal cliff located approximately 10 km northeast of the city of Nelson on the South Island of New Zealand (Figure 1). Rocks eroded from the cliffs of McKay Bluff are considered to have contributed to the distinctive boulder bank that continues for approximately 13 km from the southern end of the bluff and forms a barrier separating the estuary, Nelson Haven, from Tasman Bay (Figure 1). Studies of the formation of the Nelson Boulder Bank have been published by Dickinson and Woolfe (1997), Johnston (2001), Hartstein and Dickinson (2001) and the geological background of the location is well documented in those works. An analysis of the wave energy in Tasman Bay, to which the cliffs of McKay Bluff are exposed, is provided by Hartstein and Dickinson (2006).

2.2 Rock Slope Characteristics

The slope described in this study comprises approximately 1000 m of Cable Granodiorite exposed along the coast (Figure 1). The mineral proportions and density of granodiorite are well defined and the average density of granodiorite has been taken as 2.73 g/cm³ (AusIMM, 1995).

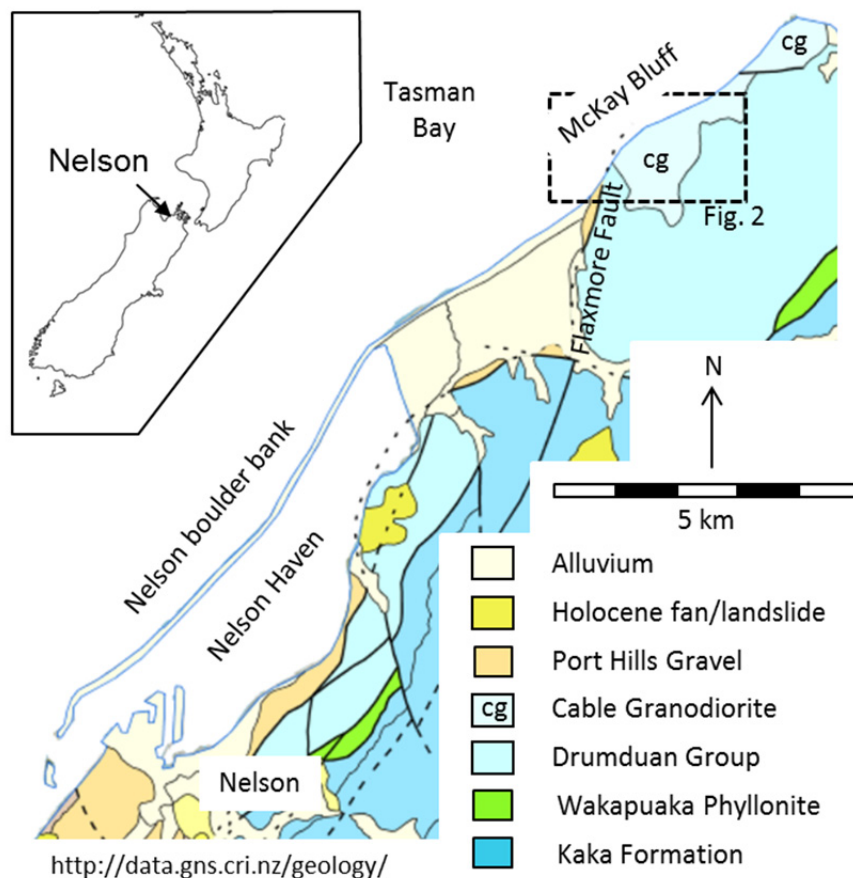


Figure 1. Location and geology map of McKay Bluff and the Nelson boulder bank, South Island New Zealand

Field data were collected from rock outcrops at five locations along the base of the slope (Figure 2, Table 1). At the northeastern end of this transect the coast makes a gentle convex bend to the east such that photographs along the coast can show a true profile of the slope (Figure 2 & 3).

McKay Bluff rises to a height of over 400 m above sea level and has a slope angle approximating 50° at its base and approximating 45° for a height of over 300 m (Figure 3). The base of the cliff is constantly being undercut by marine erosion and it is assumed the observed slope represents equilibrium between the active subaerial slope processes and the geological conditions in the slope. McKay Bluff provides an opportunity to study a high, steep slope and to investigate the mechanisms of slope instability.

2.3 Intact Rock Strength

The intact rock strength was measured using a Schmidt hammer which records the rebound of an impacting weight. The instrument used was a Proquest Rock Schmidt with an impact energy of 2.207 Nm. The instrument was used according to the International Society for Rock Mechanics (ISRM) recommended method which involves taking an average of 20 readings to derive each strength value (ISRM, 1987). Schmidt hammer rebound values (R) can be correlated with uniaxial compressive strength (UCS) and the elastic modulus (Katz, Reches, & Roegiers, 2000). A total of seven strength measurements were collected at the five locations (Table 2). The correlated UCS and elastic modulus of the rock are given in Table 2. The data on which the correlation is based does not support extrapolation above 300 MPa (Katz et al., 2000).

2.4 Rock Mass Characteristics

The joint spacing was measured at each of the five locations by counting the number of joints intersecting reference lines. At each location three, 2 meter long, reference lines oriented vertically and in two mutually perpendicular horizontal directions were used for joint spacing measurement. These data and the calculated volumetric joint count (Palmstrom, 2005) and block volume are provided in Table 1.

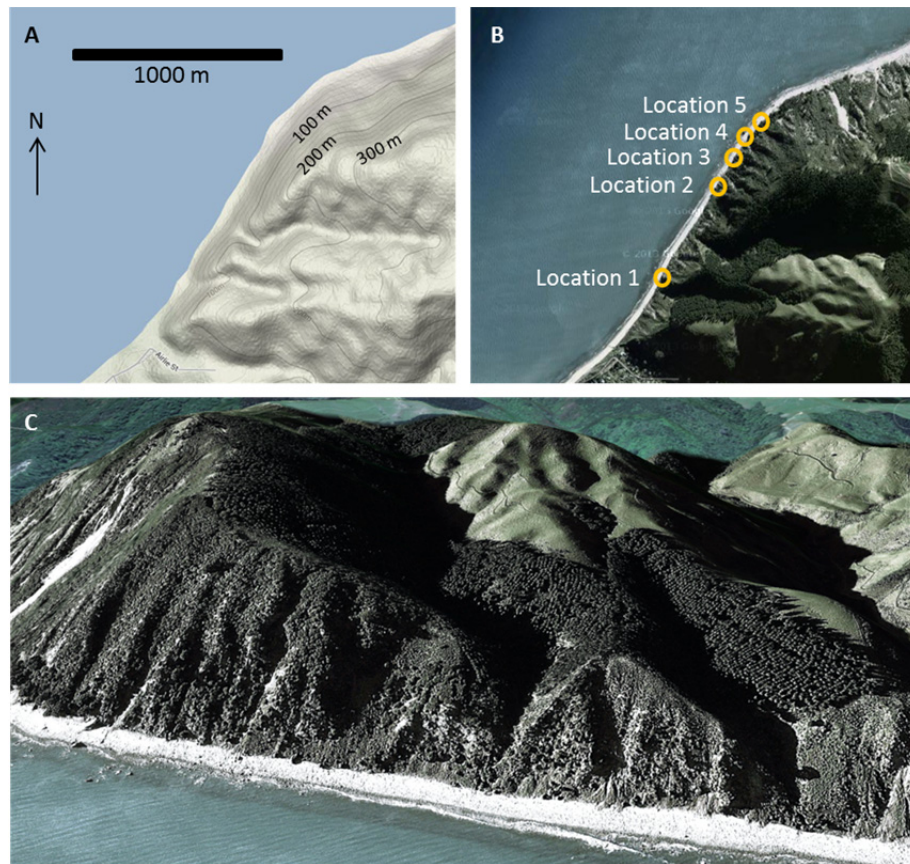


Figure 2. Topographic map satellite image and synthetic aerial view of the slopes at McKay Bluff (viewed toward the east). Google Earth (2008). Locations 1-5 referred to in the text are marked



Figure 3. Photograph of the slopes at McKay Bluff (viewed toward the north)

Table 1. Field locations (using hand-held GPS) and joint spacing data

Location	South	East	Average joints/m	Volumetric joint count	Block volume dm ³
1	41.18015	173.36762	4.3	8.7	41.5
2	41.17644	173.37077	4.5	9.0	37.0
3	41.17527	173.37172	4.8	9.7	29.9
4	41.17435	173.37229	4.0	8.0	52.7
5	41.17345	173.37367	3.5	7.0	78.7

Table 2. Field data on intact rock strength (Schmidt Hammer) following ISRM (1987) recommended method of 20 readings per UCS value. UCS and elastic modulus correlations are from Katz et al. (2000)

Location	Rebound number (R)	R standard deviation	UCS (MPa)	Elastic Modulus GPa	Comment
1	66	5.8	184	55	Red oxidized blocky rock
1	66.5	4.8	190	56	Green blocky rock
2	65.5	3.1	178	53	
3	69	7.3	225	63	
4	76.5	2.3	372	86	Fresh, wave-worn outcrop
5	60.5	5.6	127	42	
5	74.5	4.1	325	79	

The joints were observed to be slightly wavy on a large-scale and smooth to slightly rough on small scale observations, supported by measurement of the joint roughness coefficient using a brush-gauge profiling tool (Barton, 2013). The joint faces were slightly weathered with some being coated with a hard epidote alteration product less than 1 mm thick. At each location selected joint orientations were measured using a magnetic compass and corrected for magnetic declination of +22 degrees. A total of 60 joint measurements were made.

2.5 Rock Mass Strength

The Hoek-Brown rock mass strength criterion is a methodology used for determining the strength of a rock mass based mainly on field observations (Hoek & Brown, 1997; Marinos et al., 2005). The Hoek-Brown rock mass strength criterion is based on the uniaxial compressive strength (UCS), the intact rock property value (m_i) and the Geological Strength Index (GSI). It is rare for a rock mass to have a unique strength value and it is common to consider a range of values (Hoek & Brown, 1997). In particular, the GSI value was intended to be assessed visually and not considered in divisions below 5 points (Hoek & Brown, 1997; Marinos et al., 2005). Visual field assessment, joint spacing measurements and stereographic analysis of the joint orientations identified the rock mass as 'blocky' in the GSI framework ("very well interlocked undisturbed rock mass consisting of cubical blocks formed by three orthogonal discontinuity sets") with 'fair' joint conditions ("smooth moderately weathered or altered surfaces"). Other authors have provided quantitative guides for GSI (e.g. Cai, Kaiser, Uno, Tasaka, & Minami, 2004). Using the spacing and block volume measurements (Table 1) and a joint condition rating of fair a representative range of GSI from 45 to 55 was obtained. These parameters were applied to derive a range of rock mass strength values (RocLab, version 1.033, RocScience, Table 3, Figure 4).

The rock mass strength parameter used in this study is the unconfined rock mass strength which is applicable to the stress conditions near the slope face. Other strength parameters are used to assess the strength deeper into the slope such as the global rock mass strength which is higher and includes the effect of confining stress within the slope (Hoek, 2005).

Table 3. Representative rock mass strength parameters derived using the Hoek-Brown criterion (RocLab, V 1.033, RocScience)

Parameter	Low	High
<i>RocLab Inputs</i>		
Uniaxial compressive strength of intact rock, UCS (MPa)	125	250
Hoek-Brown parameter, m_i	29	29
Elasticity of intact rock, E_i (GPa)	43.1	66.4
Unit weight (kN/m^3)	26	26
Geological Strength Index, GSI	45	55
Poissons Ratio	0.3	0.3
Peak m_b	4.067	5.813
Peak s	0.0022	0.0067
Residual m_b	1	1
Residual s	0.001	0.001
<i>RockLab Outputs</i>		
Uniaxial rock mass compressive strength(MPa)	5.6	20.1
Rock mass modulus (GPa)	9.63	27.13

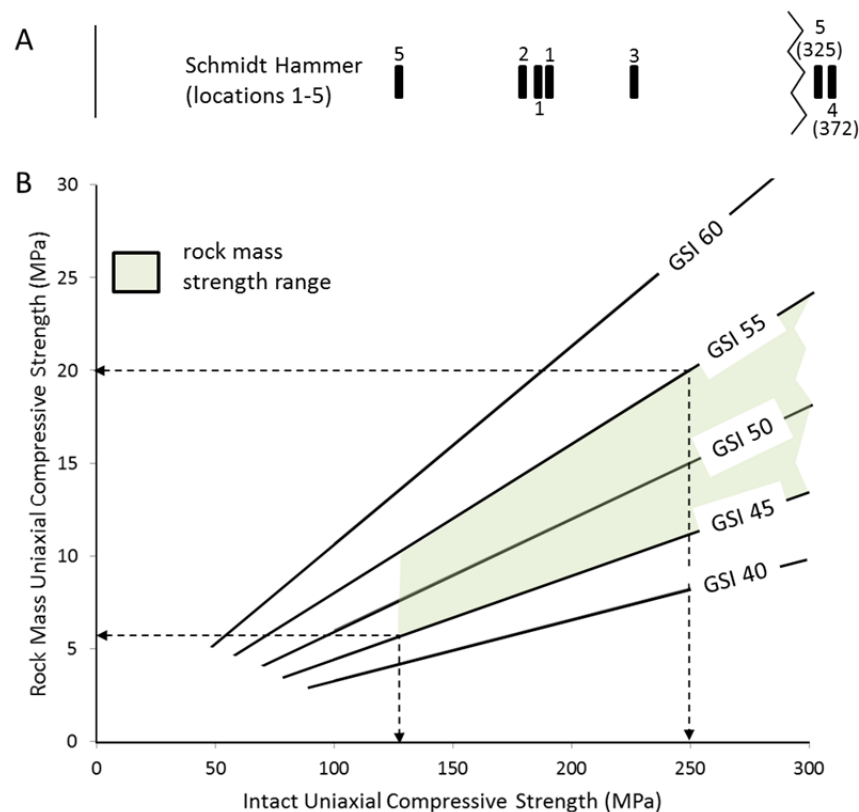


Figure 4. (A) Intact uniaxial compressive strength determined in the field by Schmidt hammer (scale at base of B. (B) Graph of rock mass uniaxial compressive strength (Rocscience RocLab V 1.033) for selected values of Geological Strength Index (GSI) versus uniaxial compressive strength range

2.6 Rock Slope Kinematics

The rocky outcrops on the slope face are of variable steepness and are locally affected by small-scale (<10 m) blocky failure zones. Some of these rocky outcrops are affected by wedge sliding failure formed by intersecting discontinuity planes (Figure 5). Blocky failure zones are also formed by the release of blocks on planes dipping steeply into the face (Figure 6). These failures can be described as toppling wedges as the steeply dipping planes allow the release of blocks from the slope.

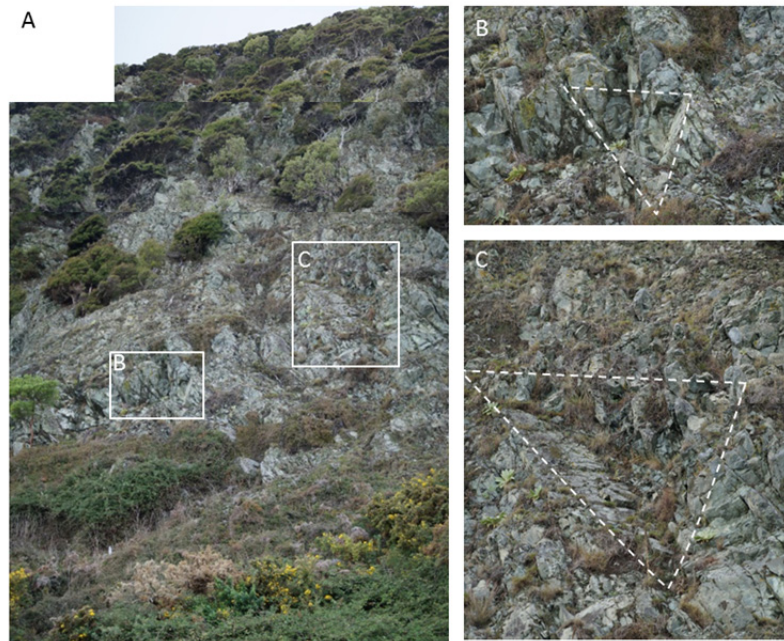


Figure 5. (A) Rocky outcrop approximately 10 m above beach level. (B and C) Sliding wedges (field of view 3 m across)



Figure 6. (A) Debris fan and rocky outcrop (viewed toward south). (B) Multiple toppling wedges (field of view 6 m across)

The active nature of these erosion mechanisms can be observed by the relatively fresh appearance of some wedge scars on the rock face and the presence of open cracks observed on the rock face. Such structural failures can occur in conditions of stress below or above the rock mass strength. If such structural failure processes are highly active it is possible that they will reduce the slope steepness to the extent that the stress in the slope is well below the rock mass strength. The cause of such structural instability must be assessed carefully, it has been proposed that some structural failure assumed to be directly gravity driven could be stress-induced (Smith 2014).

2.7 Rock Slope Stress

Stress is a three-dimensional tensor which is difficult to measure but deceptively easy to model. Stress in a slope is the distribution of forces, primarily due to gravity, through the topography. The fundamental controls on stress include density of the rock, height of the slope and steepness of the slope. Other factors also need to be considered (Table 4). Due to tectonic processes additional forces, typically horizontal, contribute to the total stress pattern. The World Stress Map (Heidbach, Tingay, Barth, Reinecker, Kurfeß, & Müller, 2008) provides a compendium of stress measurements from a range of sources. The nearest high quality reading to the site is an earthquake focal mechanism interpretation approximately 100 km southwest of the site. At that site the maximum stress is horizontal compression oriented west-northwest. This maximum compression direction is corroborated by other data from around the region (Heidbach et al., 2008).

Another influence is that stress cannot exceed the strength of the rock and the rock fails or yields where stress reaches equivalence with the strength. Where local failure or yielding occurs, stress is redistributed to surrounding parts of the rock. The presence of water also plays an important role in slope stability as the pore pressure impacts on rock and soil strength.

A finite element modeling software package has been used to provide a range of stress analyses in slopes and to assess sensitivities (Phase2, V. 8.020, RocScience). Finite element modeling (FEM) divides a two-dimensional area or three-dimensional volume into a mesh of polyhedral elements. Three-dimensional FEM is commonly available, however, two-dimensional FEM can give results that are comparable to three-dimensional analysis in situations where the geometry remains relatively consistent in the out-of-plane direction and the rockmass can be considered homogeneous and isotropic.

The FEM package solves the stress magnitude and orientation for each element providing a continuous stress model with a resolution dependent on the fineness of the mesh. Greater resolution can be achieved at the expense of longer computing times. The mesh size therefore represents a smoothing effect which must be taken into account when maximum or minimum stress values are quoted. The FEM can be interrogated to provide precise values but these values will vary depending on the mesh type and size.

A series of FEM stress analyses were conducted (Phase 2 V. 8.020, Rocscience) to illustrate difficulties in establishing meaningful results. The first and second models (Table 5) illustrate the sensitivity to the proximity of the area of interest in the model (in this case the slope and its base in particular) to the model boundary. Models 2, 3 and 4 (Table 5) show that where an angular corner exists in a model, increasing the resolution of the analytical mesh (i.e. reducing the element size) can result in great differences in maximum stress values.

Models 5 and 6 (Table 5) show the application of an inferred three-dimensional stress distribution with a maximum compression across the slope, an intermediate compression along the slope and the minimum stress being vertical (thrust faulting pattern). It can be seen that the stress ratio greatly influences the maximum stress compared to the equivalent isotropic model (Model 2 & 3, Table 5). Models 5 and 6 (Table 5) also illustrate the sensitivity to increasing resolution of the model (Figure 7A & B).

Models 7, 8 and 9 (Table 5) show the effect of smoothing the angular base of the slope with reference to isotropic stress conditions (Model 7) and an inferred stress condition range at the site (Models 8 & 9). Models 10, 11 and 12 (Table 5) have an increased radius of curvature at the base compared to the previous models. These models show a drop in stress at the base of the slope. The high stresses are still present but they are now separated from the surface by a low stress zone (Figure 7C). The low stress zone is caused by the mis-match between the applied stresses and the curvature of the slope. The phenomenon is well known in stress around tunnels in which good matching of curvature to stress conditions (e.g. circular in isotropic conditions or elliptical in non-isotropic stress conditions) is known to provide an even distribution of stress (Brady & Brown, 1993, Ren, Zuo, Xie, & Smith, 2014).

Table 4. Factors considered in assessing stress in slopes

Factor	Field data	Modeling	McKay Bluff, NZ
Slope height	Surveys	Model geometry	Approx 400 m total, main steep slope 200-300 m high.
Slope steepness	Surveys	Model geometry	Approx. 50° flattening progressively upward
Rock density	Laboratory measurement, assessment from mineral content, affected by void space	Material input	Granodiorite, mineral proportions and density well defined. Minimal reduction by fractures and voids
3D stress state including tectonic forces	Inferred from earthquakes and other field data	Adjust ratio of vertical and horizontal stress components. 2D models can incorporate through adjusting out-of-plane stress	Thrust tectonic regime. Nearest published stress data 100 km southwest. Horizontal compressive stress component across slope is maximum. Vertical stress component is minimum (thrust fault regime)
Yielding of rock	Rock mass strength assessment using engineering geology methods	Elastic models have no yielding and therefore can develop false high stress. Plastic models include yield but residual strength values poorly known	Elastic stress for the slope geometry exceeds rock mass strength. Further assessed through plastic strength models.
Structural failures	Sliding and toppling of blocks which can occur below rock mass strength	These mechanisms are modeled by limit-equilibrium and kinematic methods	Sliding and toppling wedge blocks observed
Water	Observations (e.g. springs), water table measurements	Water table surface or transient flow models	Wet, drained conditions
External loads	Sediments, engineering works, earthquakes	Model as overlying material or directly as applied distributed forces. Earthquakes modeled pseudo-statically as horizontal acceleration	Coastal sediment – load is very low compared to stresses in rock
Stress concentration	Local shape changes such as angularity or curvature of slope base. Local yielding to self-modify shape may occur.	Can impact on ‘maximum’ stress values observed at model surface. Extreme high magnitude can occur at corners. Unexpected low values can occur on curves	Slope base covered by sediment. No evidence of stress-induced concavity at base
Model boundary effects and mesh resolution	NA	Features of interest in model should be adequately distant from boundaries (e.g. 2 times slope height). Stress values measured can be highly sensitive to the model resolution. Coarse mesh models smooth stress concentration effects	Examples described in text

Models 1 to 12 (Table 5) are all based on elastic material properties. The deficiency of elastic models is that they can report stresses which are far higher than the strength of the rock mass. For an elastic model it is necessary and useful to observe the locations where the stress has exceeded the material strength. Once plastic properties are incorporated in the model these selected properties create a feedback to the stress conditions and it is possible to misinterpret whether the material has limited the stress or the stress is coincidentally equivalent to the strength.

Models 13 and 14 (Table 5) apply plastic strength behaviour based on a low and high strength condition, respectively (Table 3). The stress conditions are equivalent to model 8 (Table 5) and the base of the slope of the three models is shown for comparison in Figure 8. Not surprisingly, the material has locally yielded causing significant changes to the stress patterns (Figure 8 B & C). The limit to the zone of intense yielding corresponds to the unconfined compressive strength of the materials (5.6 MPa & 20 MPa, respectively). This correspondence is also shown on Figure 4. This example illustrates the important point that for plastic materials the strength and stress are very intimately related.

The local stress reduction (Figure 8 B & C) indicates that local yielding or failure has occurred near the face of the slope. The yielded part of the rock mass no longer carries stress and consequently, the maximum stress magnitude at the surface (as listed in Table 5) is located above and/or below the yielded portion of the slope face.



Figure 7. Finite element model (Phase 2 V. 8.020, Rocscience) illustrating differences in stress analysis for (A) an angular base with element size of approximately 5 m, (B) an angular base with element size of approximately 1.5 m and (C) a smooth shape at the base of a slope (radius of curvature approximately 50 m). The FEM output shows shaded contours of the magnitude of the maximum principal compressive stress with selected contours labelled (MPa)

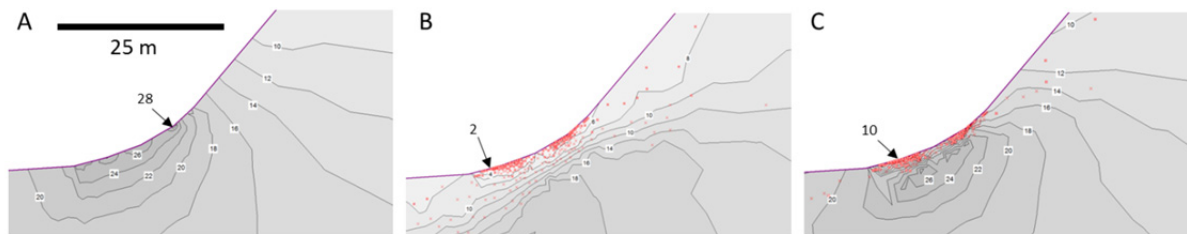


Figure 8. Finite element model (Phase 2 V. 8.020, Rocscience) illustrating differences in stress analysis for radius of curvature approximately 25 m. (A) Elastic material, (B) plastic material with low strength properties and (C) plastic material with low strength properties. Yielded elements shown as red symbols. See Table 3 for low and high strength properties. The FEM output shows shaded contours of the magnitude of the maximum principal compressive stress with selected contours labelled (MPa)

Table 5. Stress in a numerical model slope 400m high approximately 50° slope, 2D model with out-of-plane stress adjustments (V=vertical stress, Hp=horizontal stress parallel to slope, Ht=horizontal stress transverse to slope). (Phase2, V. 8.020, RocScience)

No.	Distance to model boundary relative to slope height	Approx. Element size at base (m)	Shape at base (radius of curvature, m)	3D stress V:Hp:Ht	Material type	Max. surface stress (MPa)	Comment
1	1	5	angular	isotropic	elastic	5	Poor model dimensions “Maximum stress” related to mesh density (i.e. resolution) (Figure 7A) (Figure 7B)
2	>2	5	angular	isotropic	elastic	9	
3	>2	1.5	angular	isotropic	elastic	16	
4	>2	0.5	angular	isotropic	elastic	28	
5	>2	5	angular	1:1.5:2.5	elastic	24	
6	>2	1.5	angular	1:1.5:2.5	elastic	34	Figure 8A
7	>2	1.5	25	isotropic	elastic	11	
8	>2	1.5	25	1:1:2	elastic	28	
9	>2	1.5	25	1:1.5:2.5	elastic	30	
10	>2	1.5	50	isotropic	elastic	11	
11	>2	1.5	50	1:1:2	elastic	7	Near-surface unloading at base due to shape. Minimum surface stress 4 MPa, 19 MPa at 3m below surface
12	>2	1.5	50	1:1.5:2.5	elastic	6	Near-surface unloading at base due to shape. Minimum surface stress 3 MPa, 20 MPa at 5m below surface (Figure 7C)
13	>2	1.5	25	1:1:2	plastic	8	Low strength yielding at approx. 6 MPa. Minimum surface stress at base 2 MPa (Figure 8B)
14	>2	1.5	25	1:1:2	plastic	20	High strength yielding at approx. 20 MPa. Minimum surface stress at base 10 MPa (Figure 8C)

3. Discussion

Based on the field investigations and finite element modeling, it has been possible to bracket the range of strength of the rock mass. It is likely that the rock mass does not have a unique strength but has parts which cover this range. It has also been possible to derive expected stress conditions although the values are highly sensitive to curvature of the slope base (concealed by debris) and the three-dimensional stress regime (inferred only from published records a significant distance away). By considering low and high strength values in the inferred strength range it has been possible to assess the possible extent of yielding where stress is highest (base of the slope). In this way, the likely strength and stress conditions in the slope, while not necessarily ‘determined’, have been bracketed to a satisfactory level of detail for the aims of this study – which was to illustrate the interaction of the parameters. Clearly, the resources committed to data collection and modeling can be great and depend on the expected benefits of more precise estimates.

More generally, Kennedy and Dickson (2007) showed steep slope profile shapes representative of the relative efficiency of marine and sub-aerial erosion processes (Figure 9). It is understood that the profiles presented by Kennedy and Dickson (2007) are illustrative only. However, they form a useful framework for demonstrating the range of stress distributions which may occur in such slopes. In general, the magnitude of stress developed in a

slope is proportional to the height and steepness of the slope (Table 6). The stress is also sensitive to the density of the rock mass and the three-dimensional stress conditions. Three of the illustrated profiles have an angular base which results in extremely high stress values in a high resolution elastic FEM model. In nature, it is expected that high stress would cause yielding of the material that would allow erosion of the slope to a less angular shape. Therefore determining the true maximum state of stress in a slope requires very detailed surveying of the slope shape, particularly at the base. However, the base of a slope is often concealed by debris making such surveying difficult. As an approximation to the maximum stress in slopes of the height and steepness shown in Figure 9, the results from the FEM model with coarse mesh at the toe (approximately 5 m across) can be considered as an initial guide. The models used elastic material properties and therefore the stress values are independent of the material strength. The stress values derived in these simple models can be compared to the strength of material to determine what form of strength-stress interaction is to be expected. If the elastic stress values are well below the rock mass strength then it is likely that stress-induced failures will not be significant. It would also be likely that the active erosional processes would be directly gravity driven and possibly structural in nature, such as block sliding or toppling. If the stress values are similar to, or above, the rock mass strength then plastic strength models should be applied to determine the zones of yielding. Zones of yielding in a model can be compared to the shape of the landform to validate the strength, as the yielded material is likely to have been eroded – leading to a change of shape and therefore a further change in stress.

Table 6. Stress in numerical model slopes (based on representative types of Kennedy and Dickson 2007). Analysis elements approx. 5m at base, stress isotropic, elastic material, unit weight 29 kN/m³. (Phase2, V. 8.020, RocScience)

Type	Height (m)	Max. slope angle (degrees)	Shape at base	Approximate max. stress (MPa)
Vertical	200	86	angular	8
Vertical	400	86	angular	16
Extremely steep	200	79	angular	7
Extremely steep	400	79	angular	14
Very steep	200	71	angular	5
Very steep	400	71	angular	10
Steep	200	60	smooth	3
Steep	400	60	smooth	6

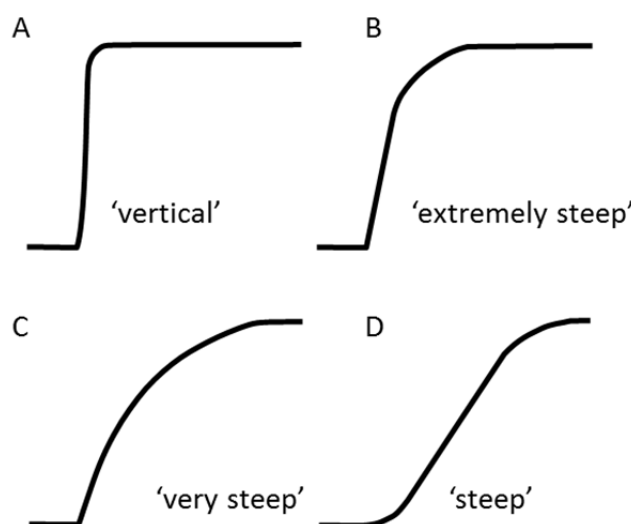


Figure 9. Coastal slope profile types with relative contribution of marine versus sub-aerial erosion decreasing from A to D (Kennedy and Dickson 2007). Short-hand names used for each type in this paper are in inverted commas

4. Conclusions

The stress in a slope is directly related to the height and steepness of the slope. The force of gravity is distributed through the rock mass as stress which increases in magnitude with the height and steepness of the landform profile. Where the strength of the rock is exceeded by the stress, the rock locally yields. This yielding or failure limits the magnitude of the stress that can develop in the slope. Also, local yielding weakens the rock and promotes reduction of slope angle and slope height through erosion and therefore reduces the stress in the slope. It is expected that the landform profiles of actively eroding natural coastal slopes represent the interplay of stress (controlled by height, steepness, rock density and limited by yield strength) and strength (controlled by the strength of the rock material and by the character and orientation of discontinuities in the rock mass). The stress in a slope can be estimated by finite element modeling however, the results are highly sensitive to a range of factors. The strength of a rock mass can be estimated using engineering geological methods but is expected to be a range rather than a unique value.

High, steep coastal cliffs at McKay Bluff near Nelson on the South Island of New Zealand have stress levels comparable to the range of strength of the rock mass. The lower end of strength estimates is likely to result in local yielding of the rock mass. The higher end estimates exceed the stress in the slope and slope failure mechanisms in these materials would be gravity-controlled structural sliding and toppling rather than stress-induced yielding.

Acknowledgments

The research was supported by RMIT University.

References

- Alejano, L. R., Gómez Márquez, I., & Martínez Alegría, R. (2010). Analysis of a complex toppling-circular slope failure. *Engineering Geology*, 114, 93-104.
- AusIMM. (1995). *Field geologists manual*. Australasian Institute of Mining and Metallurgy.
- Barton, N. (2013). Shear strength criteria for rock, rock joints, rockfill and rock masses: Problems and some solutions. *Journal of Rock Mechanics and Geotechnical Engineering*, 5, 249-261.
- Brady, B. H. G., & Brown, E. T. (1993). *Rock mechanics for underground mining*, Chapman and Hall.
- Brideau, M. A., Yan, M., & Stead, D. (2009). The role of tectonic damage and brittle rock fracture in the development of large rock slope failures. *Geomorphology*, 103, 30-49.
- Cai, M., Kaiser, P. K., Uno, H., Tasaka, Y., & Minami, M. (2004). Estimation of rock mass deformation modulus and strength of jointed hard rock masses using the GSI system. *International Journal of Rock Mechanics & Mining Sciences*, 41, 3-19.
- Delgado, J., Vicente, F., García Tortosa, F., Alfaro, P., Estévez, A., López Sánchez, J. M., & Mallorquí, J. J. (2011). A deep seated compound rotational rock slide and rock spread in SE Spain: Structural control and DInSAR monitoring. *Geomorphology*, 129, 252-262.
- Dickinson, W. W., & Woolfe, K. J. (1997). An in-situ transgressive barrier model for the Nelson Boulder Bank New Zealand. *Journal of Coastal Research*, 13, 937-952.
- Gómez Pujol, L., Gelabert, B., Fornós, J. J., Pardo Pascual, J. E., Rosselló, V. M., Segura, F. S., & Onac, B. P. (2013). Structural control on the presence and character of calas: Observations from Balearic Islands limestone rock coast macroforms. *Geomorphology*, 194, 1-15.
- Google Earth 6.0. (2014). Retrieved August 31, 2014, from <http://www.google.com/earth/index.html>
- Hartstein, N. D., & Dickinson, W. W. (2001). Gravel Barrier Migration and Overstepping in Cable Bay Nelson New Zealand. *Journal of Coastal Research*, 34, 256-266.
- Hartstein, N. D., & Dickinson, W. W. (2006). Wave energy and clast transport in eastern Tasman Bay New Zealand. *Earth Surface Processes and Landforms*, 31, 703-714.
- Heidbach, O., Tingay, M., Barth, A., Reinecker, J., Kurfes, D., & Müller, B. (2008). The World Stress Map database release. <http://dx.doi.org/10.1594/GFZ.WSM.Rel2008>, 2008
- Hoek, E. (2005). Uniaxial compressive strength versus Global strength in the Hoek-Brown criterion Evert Hoek Vancouver. Retrieved March 30, 2005, from <http://www.wrocscience.com/library/rocnews/Spring2005.htm> accessed 17/7/2013
- Hoek, E., & Brown, E. T. (1997). Practical Estimates of Rock Mass Strength. *International Journal of Rock*

- Mechanics and Mining Sciences*, 34, 1165-1186.
- ISRM. (1987). Suggested methods for determining hardness and abrasiveness of rocks. *International Journal of Rock Mechanics and Mining Sciences & Geomechanical Abstracts*, 15, 89-97.
- Johnston, M. R. (2001). Nelson Boulder Bank, New Zealand. *New Zealand Journal of Geology and Geophysics*, 44, 79-88.
- Katz, O., Reches, Z., & Roegiers, J. C. (2000). Evaluation of mechanical rock properties using a Schmidt Hammer. *International Journal of Rock Mechanics and Mining Sciences*, 37, 723-728.
- Kinakin, D., & Stead, D. (2005). Analysis of the distributions of stress in natural ridge forms: implications for the deformation mechanisms of rock slopes and the formation of sackung. *Geomorphology*, 65, 85-100.
- Korup, O. (2004). Geomorphic implications of fault zone weakening: slope instability along the Alpine Fault South Westland to Fiordland. *New Zealand Journal of Geology and Geophysics*, 47, 257-267.
- Marinos, V., Marinos, P., & Hoek, E. (2005). The geological strength index: applications and limitations. *Bulletin of Engineering Geology and Environment*, 64, 55-65.
- Naylor, L. A., & Stephenson, W. J. (2010). On the role of discontinuities in mediating shore platform erosion. *Geomorphology*, 114, 89-100.
- Naylor, L. A., Stephenson, W. J., & Trenhaile, A. S. (2010). Rock coast geomorphology: recent advances and future research directions. *Geomorphology*, 114, 3-11.
- Palmstrom, A. (2005). Measurements of and correlations between block size and rock quality designation (RQD). *Tunnelling and Underground Space Technology*, 20, 362-377.
- Paterson, M. S., & Wong, T. F. (2005). Experimental rock deformation: the brittle field. *Springer*, 314.
- Ren, G., Zuo, Z. H., Xie, Y. M., & Smith, J. V. (2014). Underground excavation shape optimization considering material nonlinearities. *Computers and Geotechnics*, 58, 81-87.
- Smith, J. V. (2014). A new approach to kinematic analysis of stress-induced structural slope instability. *Engineering Geology*, 394. <http://dx.doi.org/10.1016/j.enggeo.2014.12.015>
- Stead, D., Eberhardt, E., & Coggan, J. S. (2006). Developments in the characterization of complex rock slope deformation and failure using numerical modeling techniques. *Engineering Geology*, 83, 217-235.
- Stephenson, W. J., & Naylor, L. A. (2011). Geological controls on boulder production in a rock coast setting: insights from South Wales UK. *Marine Geology*, 283, 12-24.
- Wyllie, D. C., & Mah, C. (2004). *Rock slope engineering*. Taylor & Francis.
- Youssef, A. M., Maerz, N. H., & Al Otaibi, A. A. (2012). Stability of rock slopes along Raidah escarpment road, Asir Area, Kingdom of Saudi Arabia. *Journal of Geography and Geology*, 4(2), 48.

Copyrights

Copyright for this article is retained by the author(s), with first publication rights granted to the journal.

This is an open-access article distributed under the terms and conditions of the Creative Commons Attribution license (<http://creativecommons.org/licenses/by/3.0/>).